Available online at www.sciencedirect.com
ScienceDirect
Ceramics International 35 (2009) 3395–3400
CERAMICS INTERNATIONAL
www.elsevier.com/locate/ceramint

Mechanical properties and rapid consolidation of binderless nanostructured tantalum carbide

Byung-Ryang Kim [a], Kee-Do Woo [a,b], Jung-Mann Doh [c], Jin-Kook Yoon [c], In-Jin Shon [a,b,*]

[a] Division of Advanced Materials Engineering and the Research Center of Advanced Materials Development, Engineering College, Chonbuk National University, 561-756, Republic of Korea
[b] Department of Hydrogen and Fuel Cells Engineering, Specialized Graduate School, Chonbuk National University, 561-756, Republic of Korea
[c] Advanced Functional Materials Research Center, Korea Institute of Science and Technology, PO Box 131, Cheongryang, Seoul 130-650, Republic of Korea

Received 7 March 2009; received in revised form 7 May 2009; accepted 7 June 2009
Available online 7 July 2009

Abstract

The rapid sintering of nanostructured TaC hard material was investigated with a focus on the manufacturing potential of high-frequency induction heated sintering process. The advantage of this process is that it allows very quick densification to near theoretical density and prohibition of grain growth in nanostructured materials. A dense pure TaC hard material with a relative density of up to 96% was produced with simultaneous application of 80 MPa pressure and induced current within 3 min. The finer the initial TaC powder size, the higher the density and the better mechanical properties. The fracture toughness and hardness values obtained from 10 h milled powder were 5.1 ± 0.3 MPa $m^{1/2}$ and 22 GPa, respectively, under 80 MPa pressure and 80% output of total power capacity (15 kW).

Keywords: A. Sintering; B. Nanocomposites; C. Hardness; Toughness

1. Introduction

The physical and chemical properties of transition metal carbides are of interest for basic research and several technological applications. Industrial applications of the carbides are cutting tools, hard coating, and hard constituents in the metal matrix composites for high temperature applications because of their great strength, hardness and melting temperature [1–5]. Among these carbides, tantalum carbide is a very important and promising properties, such as outstanding hardness, high melting point (3880 °C), good resistance to chemical attack, thermal shock and oxidation, and excellent electronic conductivity [2,5–7].

Nanocrystalline materials have received much attention as advanced engineering materials with improved physical and mechanical properties [8,9]. As nanomaterials possess high strength, high hardness, excellent ductility and toughness, undoubtedly, more attention has been paid for the application of nanomaterials [10–12]. In recent days, nanocrystalline powders have been developed by the thermochemical and thermomechanical process named as the spray conversion process (SCP), co-precipitation and high-energy milling [13–15]. However, the grain size in sintered materials becomes much larger than that in pre-sintered powders due to a fast grain growth during the conventional sintering process. Therefore, even though the initial particle size is less than 100 nm, the grain size increases rapidly up to 500 nm or larger during the conventional sintering [16]. So, controlling grain growth during sintering is one of the keys to the commercial success of nanostructured materials. In this regard, the high-frequency induction heated sintering method (HFIHS) which can make dense materials within 2 min has been shown to be effective in achieving this goal [17–20].

In this work, we investigated the sintering of TaC without the use of a binder by the HFIHS method. The goal of this research is to produce dense binderless nanostructured TaC hard material. In addition, we also studied the effect of high-energy

* Corresponding author at: Engineering College, Chonbuk National University, Division of Advanced Materials Engineering, The Research Center of Advanced Materials Development, Jeonbuk 561-756, Republic of Korea. Tel.: +82 63 270 2381; fax: +82 63 270 2386.
E-mail address: ijshon@chonbuk.ac.kr (I.-J. Shon).

0272-8842/$36.00
doi:10.1016/j.ceramint.2009.06.012

ball milling on the sintering behavior and mechanical properties of binderless TaC.

2. Experimental procedure

The tantalum carbide powder with a grain size of −325 mesh and 99.5% purity used in this research was supplied by Alfa. The powder was first milled in a high-energy ball mill (Pulverisette-5 planetary mill) at 250 rpm for various periods of time (0, 1, 4, and 10 h). Tungsten carbide balls (8.5 mm in diameter) were used in a sealed cylindrical stainless steel vial under an argon atmosphere. The weight ratio of balls-to-powder was 30:1. Milling resulted in a significant reduction of the grain size. The grain sizes of the TaC was calculated from the full width at half-maximum (FWHM) of the diffraction peak by C. Suryanarayana and M. Grant Norton's formula [21]:

$$B_r(B_{\text{crystalline}} + B_{\text{strain}})\cos\theta = \frac{k\lambda}{L} + \eta\sin\theta \quad (1)$$

where B_r is the FWHM of the diffraction peak after instrument correction; $B_{\text{crystalline}}$ and B_{strain} are FWHM caused by small grain size and internal stress, respectively; k is a constant (with a value of 0.9); λ is the wavelength of the X-ray radiation; L and η are grain size and internal strain, respectively; θ is the Bragg angle. The parameters B and B_r follow Cauchy's form with the relationship: $B = B_r + B_s$, where B and B_s are FWHM of the broadened Bragg peaks and the standard sample's Bragg peaks, respectively. The average grain sizes of the TaC milled for 1, 4 and 10 h determined by C. Suryanarayana and M. Grant Norton's formula were about 31, 20 and 15 nm, respectively.

The powders were placed in a graphite die (outside diameter, 45 mm; inside diameter, 20 mm; height, 40 mm) and then introduced into the high-frequency induction heating sintering (HFIHS) apparatus shown schematically in Fig. 1. The HFIHS apparatus includes a 15 kW power supply which provides an induced current through the sample, and 50 kN uniaxial press.

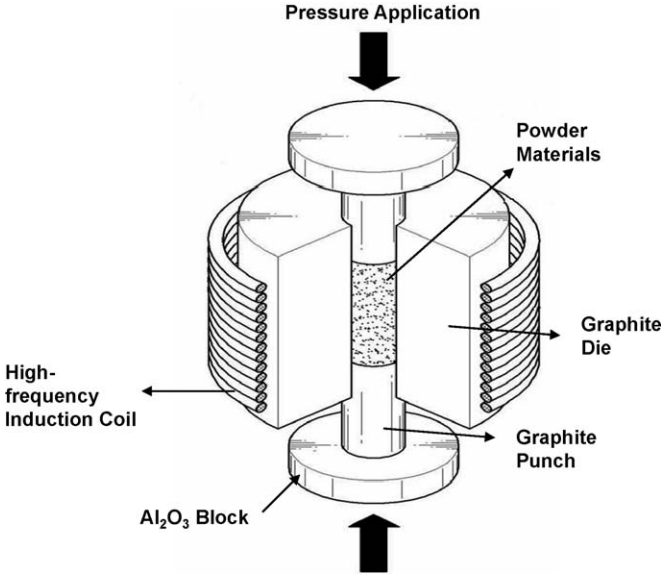

Fig. 1. Schematic diagram of the apparatus for high-frequency induction heated sintering.

The system was first evacuated and a uniaxial pressure of 80 MPa was applied. An induced current was then activated and maintained until the densification rate was negligible, as indicated by real-time output of the shrinkage of the sample. The shrinkage was measured by a linear gauge measuring the vertical displacement. The HFIHS can be controlled in two ways: by temperature control or by output control. The latter was chosen to investigate the effect of the output of total power, given that the induced current level has a direct effect on the rate of heating and on the maximum temperature. The output level was 80% output of total power. Temperatures were measured by a pyrometer focused on the surface of the graphite die. At the end of the process, the induced current was turned off and the sample cooled to room temperature. The process was carried out under a vacuum of 4×10^{-2} Torr.

The relative density of the sintered sample was measured by the Archimedes method. Microstructural information was obtained from product samples, which had been polished and etched using Murakami's reagent (10 g potassium ferricyanide, 10 g NaOH, and 100 mL water) for 1–2 min at room temperature. Compositional and microstructural analyses of the products were made through X-ray diffraction (XRD), scanning electron microscopy (SEM) with energy dispersive spectroscopy (EDS) and field emission scanning electron microscope (FE-SEM).

Vickers hardness measurements were performed on polished sections of the TaC samples using a 196 N load and 15 s dwell time. Indentations with large enough loads produced radial cracks emanating from the corners of the indent. The length of these cracks permits the fracture toughness of the material to be estimated using Anstis' expression [22]:

$$K_{\text{IC}} = 0.016\left(\frac{E}{H}\right)^{1/2}\frac{P}{C^{3/2}} \quad (2)$$

where E is Young's modulus, H is the indentation hardness, P is the indentation load, and C is the trace length of the crack measured from the center of the indentation.

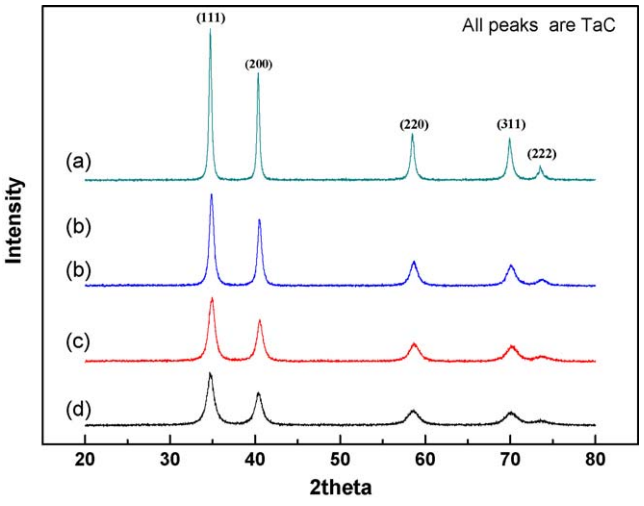

Fig. 2. X-ray diffraction patterns of the TaC powder after various milling time: (a) 0, (b) 1, (c) 4, and (d) 10 h.

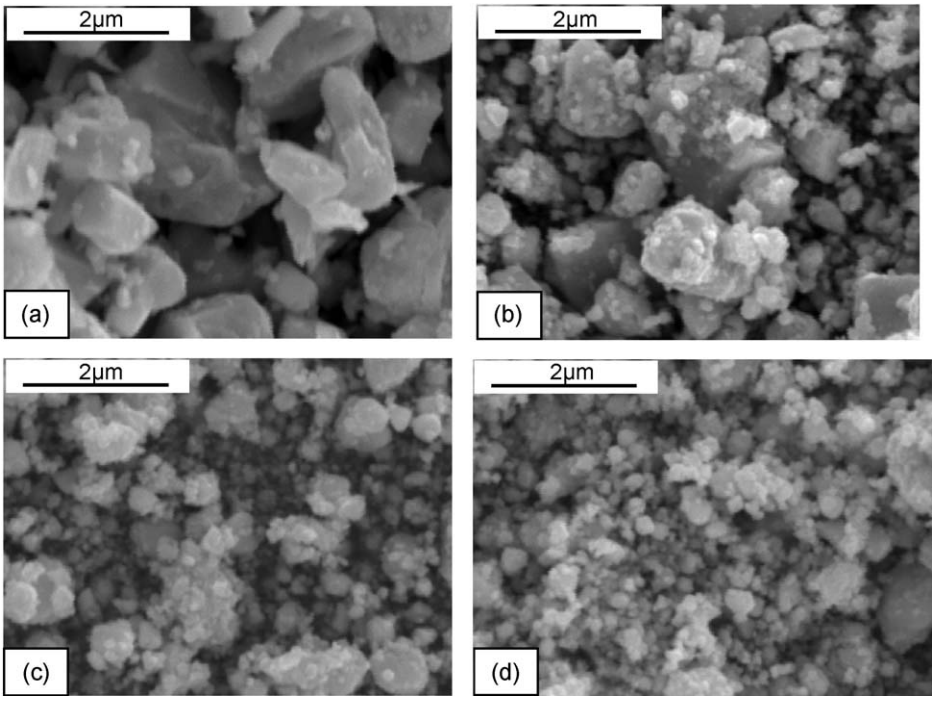

Fig. 3. SEM images of the TaC powders with milling times: (a) 0, (b) 1, (c) 4, and (d) 10 h.

3. Results and discussion

Fig. 2 shows X-ray diffraction patterns of the TaC powder after various milling time. The FWHM of the diffraction peak is wider with milling time due to the strain and the refinement of powder. SEM images of TaC powder with milling time are shown in Fig. 3. The TaC powder without milling has a angular shape but the TaC powder gets rounder shape and comes refinement with milling time. The variations of the shrinkage displacement and temperature with the heating time for 80% of the total output power capacity (15 kW) during the sintering of the high-energy ball milled TaC under a pressure of 80 MPa are shown in Fig. 4. In all cases, the application of the induced current resulted in shrinkage due to consolidation. The shrinkage initiation temperature varied from 700 to 1000 °C depending on the milling time. The temperature at which shrinkage started decreased with increasing milling time, and the high-energy ball milling affected the rate of

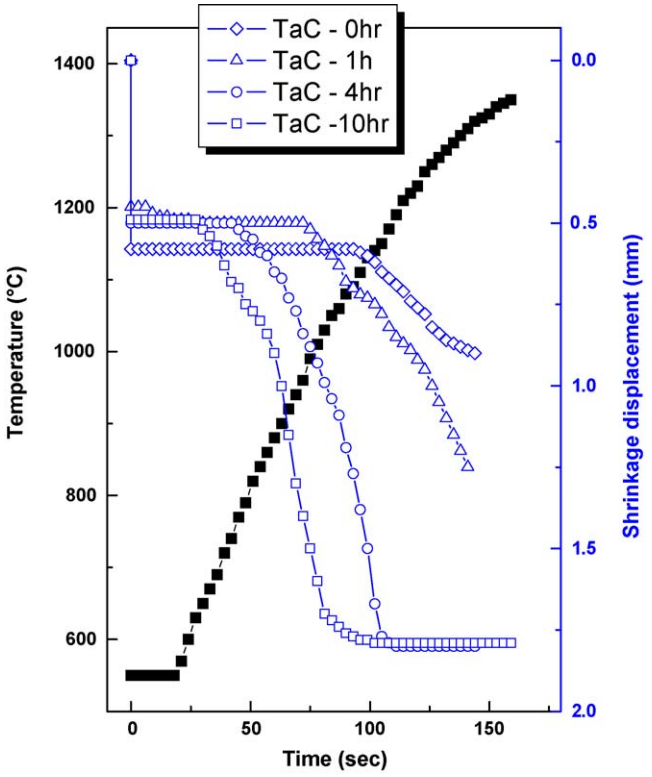

Fig. 4. Variations of temperature and shrinkage with heating time during the sintering of binderless TaC with milling times of 0, 1, 4, and 10 h.

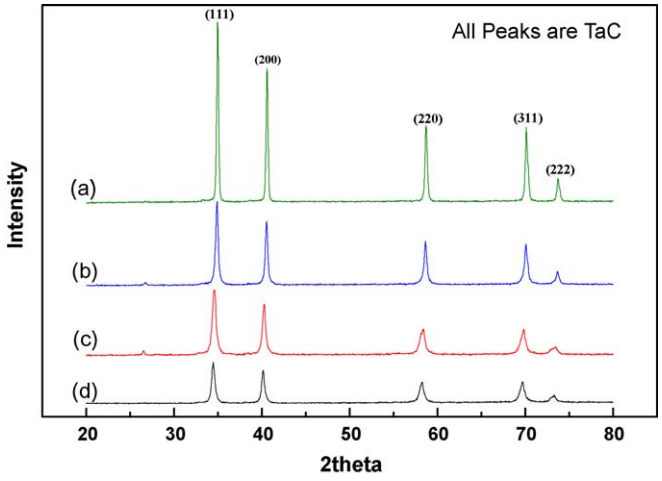

Fig. 5. XRD patterns of binderless TaC sintered from various milled powders: (a) 0, (b) 1, (c) 4, and (d) 10 h.

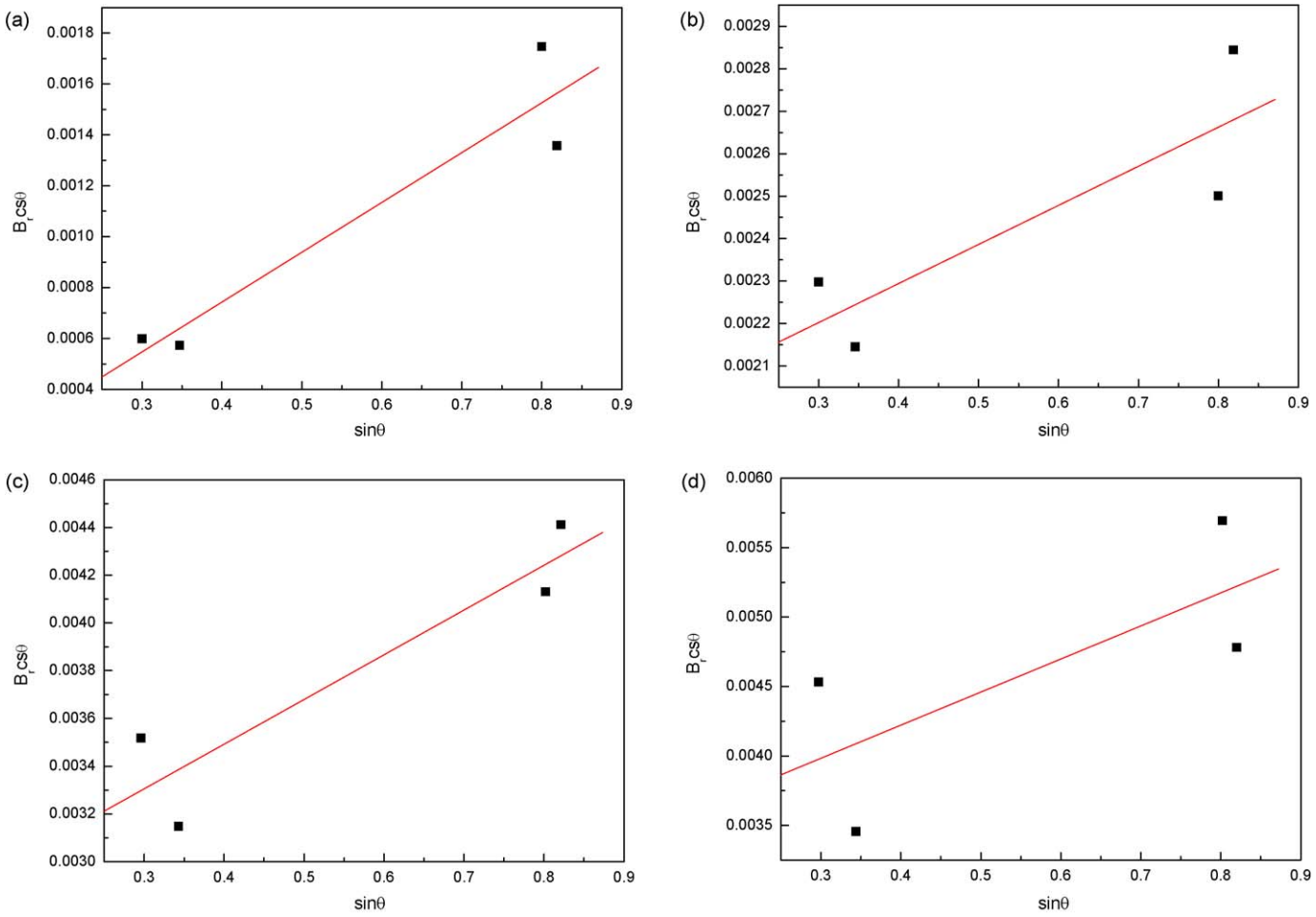

Fig. 6. Plot of B_r ($B_{\text{crystalline}} + B_{\text{strain}}$)cos θ versus sin θ for TaC sintered from various milled powders: (a) 0, (b) 1, (c) 4, and (d) 10 h.

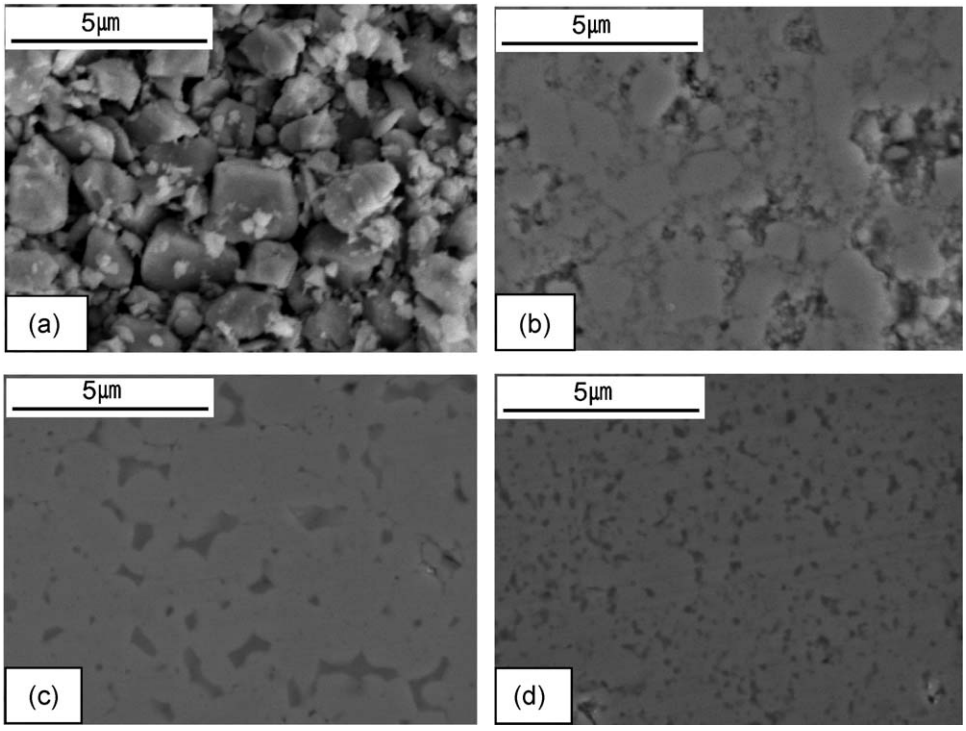

Fig. 7. SEM image of pure TaC sintered from various milled powder: (a) 0, (b) 1, (c) 4, and (d) 10 h.

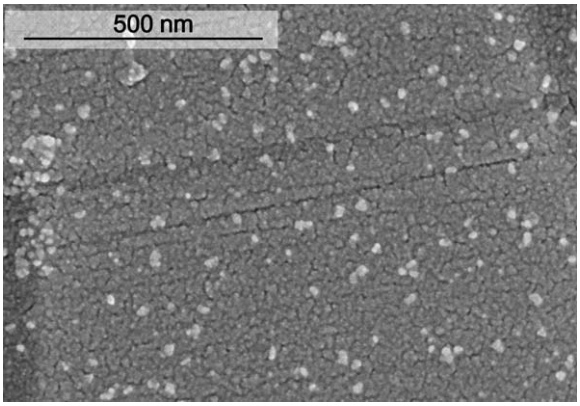

Fig. 8. FE-SEM micrographs of pure TaC sintered from the 10 h milled powder.

densification and the final density, as will be discussed below. High-energy ball milling treatment allows the control of the formation of compound by fixing the reactant powder microstructure. Indeed, high-energy ball milling produces finer crystallites, strain and defects. Therefore, consolidation temperature decreases with milling time because driving force for sintering and contact points of powders for atomic diffusion increases. Fig. 5 shows the XRD patterns of TaC sintered for all four powders used in this work. All peaks belong to TaC. A plot of B_r ($B_{\text{crystalline}} + B_{\text{strain}}$)cos θ versus sin θ [21] is shown in Fig. 6. The average grain sizes of the TaC calculated from the XRD data were about 935, 184, 72 and 33 nm for the samples with milling times of 0, 1, 4, and 10 h and their corresponding densities were approximately 68, 88, 95 and 96%, respectively. Thus, the average grain size of the sintered TaC is not greatly larger than that of the initial powder, indicating the absence of great grain growth during sintering. This retention of the grain size is attributed to the high heating rate and the relatively short term exposure of the powders to the high temperature. As the initial particle size of the TaC powder increased, the porosity also increased. Fig. 7 shows SEM image of TaC sintered from various milled powders and FE-SEM image of TaC sintered from the 10 h milled powder is shown in Fig. 8. From the figures, it becomes evident that the grain size of TaC decreases with milling time.

The role of the current (resistive or inductive) in sintering and or synthesis has been focus of several attempts aimed at providing an explanation to the observed enhancement of sintering and the improved characteristics of the products. The role played by the current has been variously interpreted, the effect being explained in terms of fast heating rate due to Joule heating, the presence of plasma in pores separating powder particles [23], and the intrinsic contribution of the current to mass transport [24–26].

The Vickers hardnesses of the TaC with ball milling for 1, 4 and 10 h were 13, 14 and 22 GPa, and their fracture toughnesses were 3.9 ± 0.3, 4.1 ± 0.4 and 5.1 ± 0.3 MPa $m^{1/2}$, respectively. These values represent the average of 10 measurements. The hardness of TaC with ball milling for 10 h is very high with high fracture toughness due to refinement of grain.

4. Summary

Using the new rapid sintering method, HFIHS, the densification of binderless TaC was accomplished using high-energy ball milling. Consolidation temperature decreased with milling time because driving force for sintering and contact points of powders for atomic diffusion increased. The average grain sizes of the TaC were about 935, 184, 72 and 33 nm for the samples with milling times of 0, 1, 4, and 10 h and their corresponding densities were approximately 68, 88, 95 and 96%, respectively. The Vickers hardnesses of the TaC with ball milling for 1, 4 and 10 h were 13, 14 and 22 GPa, and their fracture toughnesses were 3.9 ± 0.3, 4.1 ± 0.4 and 5.1 ± 0.3 MPa $m^{1/2}$, respectively.

Acknowledgement

This work was supported by a Korea Science and Engineering Foundation (KOSEF) grant funded by the Korea government (MOST) (No. R01-2007-000-20002-0).

References

[1] S.H. Jhi, S.G. Louie, M.L. Cohen, J. Ihm, Vacancy hardening and softening in transition metal carbides and nitrides, Phys. Rev. Lett. 86 (15) (2001) 3348–3351.
[2] E.K. Storms, Refractory Carbides, Academic Press, New York, 1967.
[3] L.E. Toth, Transition Metal Carbides and Nitrides, Academic Press, New York, 1971.
[4] C. Kral, W. Lengauer, D. Rafaja, P. Ettmayer, Critical review on the elastic properties of transition metal carbides, nitrides and carbonitrides, J. Alloys Compd. 265 (1988) 215–233.
[5] G.S. Upadhyaya, Nature and Properties of Refractory Carbides, Nova Science Publishers, New York, 1996.
[6] N. Ahlen, M. johnsson, M. Nygren, Oxidation behaviour of $TaTi_{1-x}C_x$ and $Ta_xTi_{1-x}C_yN_{1-y}$, Thermochim. Acta 336 (1999) 111–120.
[7] Q.w. Guo, Encyclopedia of Chemical Industry, vol. 15, Chemical Industry Press, Beijing, 1997.
[8] H. Suzuki, et al., Cemented Carbide and Sintered Hard Materials, Maruzen, Tokyo, 1986.
[9] M. Sherif El-Eskandarany, Structure and properties of nanocrystalline TiC full-density bulk alloy consolidated from mechanically reacted powders, J. Alloys Compd. 305 (2000) 225–238.
[10] L. Fu, L.H. Cao, Y.S. Fan, Two-step synthesis of nanostructured tungsten carbide-cobalt powders, Scripta Mater. 44 (2001) 1061–1068.
[11] K. Niihara, A. Nikahira, Advanced Structural Inorganic Composite, Elsevier Scientific Publishing Co., Trieste, Italy, 1990.
[12] S. Berger, R. Porat, R. Rosen, Nanocrystalline materials: a study of WC-based hard metals, Prog. Mater. 42 (1997) 311–320.
[13] Z. Fang, J.W. Eason, Study of nanostructured WC–Co composites, Int. J. Refract. Met. Hard Mater. 13 (1995) 297–303.
[14] I.J. Shon, D.K. Kim, K.T. Lee, K.S. Nam, Properties and consolidation of nanostructured $Ce_{0.8}Gd_{0.2}O_{1.9}$ by pulsed-current-activated sintering, Met. Mater. Int. 5 (2008) 593–598.
[15] I.J. Shon, D.K. Kim, I.Y. Ko, J.K. Yoon, K.T. Hong, Fabrication of nanocrystalline $TaSi_2$–SiC composite by high frequency induction heated combustion synthesis and its mechanical properties, Mater. Sci. Forum 534–536 (2007) 525–528.
[16] M. Sommer, W.D. Schubert, E. Zobetz, P. Warbichler, On the formation of very large WC crystals during sintering of ultrafine WC–Co alloys, Int. J. Refract. Met. Hard Mater. 20 (2002) 41–50.
[17] I.K. Jeong, J.H. Park, J.M. Doh, K.Y. Kim, K.D. Woo, I.Y. Ko, I.J. Shon, Mechanical properties and consolidation of ultra-fine WC–10Co and

WC–10Fe hard materials by rapid sintering process, J. Kor. Inst. Met. Mater. 46 (2008) 223–226.
[18] H.C. Kim, I.J. Shon, I.K. Jeong, I.Y. Ko, Rapid Sintering of nanocrystalline 8 mol.%Y_2O_3-stabilized ZrO_2 by high-frequency induction heating method, Met. Mater. Int. 12 (2006) 393–398.
[19] D.Y. Oh, H.C. Kim, J.K. Yoon, I.J. Shon, Simultaneous synthesis and consolidation process of ultra-fine WSi_2–SiC and its mechanical properties, J. Alloys Compd. 386 (2005) 270–275.
[20] H.C. Kim, I.J. Shon, I.K. Jeong, I.Y. Ko, J.K. Yoon, J.M. Doh, Rapid sintering of ultra fine WC and WC–Co hard materials by high-frequency induction heated sintering and their mechanical properties, Met. Mater. Int. 13 (2007) 39–45.
[21] C. Suryanarayana, M. Grant Norton, X-ray Diffraction: A Practical Approach, Plenum Press, New York, 1998.
[22] G.R. Anstis, P. Chantikul, B.R. Lawn, D.B. Marshall, A critical evaluation of indentation techniques for measuring fracture toughness. I. Direct crack measurements, J. Am. Ceram. Soc. 64 (1981) 533–538.
[23] Z. Shen, M. Johnsson, Z. Zhao, M. Nygren, Spark plasma sintering of alumina, J. Am. Ceram. Soc. 85 (2002) 1921–1927.
[24] J.E. Garay, U. Anselmi-Tamburini, Z.A. Munir, S.C. Glade, P. Asoka-Kumar, Electric current enhanced defect mobility in Ni_3Ti intermetallics, Appl. Phys. Lett. 85 (2004) 573–575.
[25] J.R. Friedman, J.E. Garay, U. Anselmi-Tamburini, Z.A. Munir, Modified interfacial reactions in Ag–Zn multilayers under the influence of high DC currents, Intermetallics 12 (2004) 589–597.
[26] J.E. Garay, J.E. Garay, U. Anselmi-Tamburini, Z.A. Munir, Enhanced growth of intermetallic phases in the Ni–Ti system by current effects, Acta Mater. 51 (2003) 4487–4495.